Marek Faryna[a,b], Waldemar Pyda[c]
[a] *Regional Laboratory of Physicochemical Analyses, Jagiellonian University, 3 Ingardena St., 30-060 Cracow, Poland*
[b] *Institute of Metallurgy and Materials Science, Polish Academy of Sciences, 25 Reymonta St., 30-059 Cracow, Poland*
[c] *AGH – University of Mining and Metallurgy, Faculty of Materials Science and Ceramics, Al. Mickiewicza 30, 30-059, Cracow, Poland*

STRUCTURAL CERAMIC COMPOSITES: PROCESSING, PROPERTIES AND ORIENTATION RELATIONSHIPS

Key words

zirconia, alumina, carbides, composites, nanocomposites, orientation imaging microscopy (OIM^{TM}), electron back scatter diffraction (EBSD), selected area diffraction (SAED), crystal structure.

Abstract

Structural ceramic matrix composites are reviewed with emphasis on the Y-TZP/Al_2O_3, Y-TZP/WC, Y-TZP/NbC, Y-TZP/TaC and Al_2O_3/WC systems. The paper is divided into to two parts. First, two processing routes for the Y-TZP/ Al_2O_3 composites containing submicronic and near-nanometric alumina particles, namely conventional powder processing and co-precipitation processing are presented in detail. The relation between mechanical properties, processing and microstructure of the composites is explored. Second, studies of crystallographic relationships between adjacent phases in the Y-TZP/WC,

Y-TZP/NbC, Y-TZP/TaC and Al_2O_3/WC systems made by using both a SEAD and EBSD method are described.

Streszczenie

Dokonano przeglądu kompozytów z osnową ceramiczną do zastosowań konstrukcyjnych kładąc nacisk na układy Y-TZP/Al_2O_3, Y-TZP/WC, Y-TZP/NbC, Y-TZP/TaC i Al_2O_3/WC. Artykuł składa się z dwóch części. W pierwszej, szczegółowo zaprezentowano dwa sposoby otrzymywania kompozytów Y-TZP/Al_2O_3 zawierających submikronowe i bliskie nanometrycznemu rozmiarowi cząstki korundu, a mianowicie wytwarzanie tradycyjne i metodę współstrącania. Zgłębiono zależność pomiędzy właściwościami mechanicznymi, sposobem wytwarzania i mikrostrukturą kompozytów. W drugiej części, opisano badania zależności krystalograficznych pomiędzy sąsiadującymi ze sobą fazami w układach Y-TZP/WC, Y-TZP/NbC, Y-TZP/TaC i Al_2O_3/WC przeprowadzone za pomocą metod SEAD i EBSD.

1. Introduction

One of the major characteristics, and simultaneously the greatest disadvantage, of ceramics is their inherent brittleness. One mechanism of overcoming this unwelcome feature of ceramics is to add a reinforcing phase and make a ceramic matrix composite. However, the reinforcements tend to hinder densification and make processing more difficult. The difficulties raise when ceramic matrix nanocomposites are produced.

In this paper, the intimate relation between the properties, processing and microstructure of ceramic matrix composites is studied. In spite of the relation is known [1], an effect of individual microstructural features on mechanical properties is sometimes underestimated or neglected. This concerns remains of porosity and accompanying processing defects.

The work is restricted to structural ceramic composites containing inclusions of submicron or near-nanometric size. Particular emphasis will be given to yttria-stabilized zirconia (Y-TZP) matrices containing alumina and carbide inclusions (WC, TaC and NbC) and to Al_2O_3 containing WC.

The Y-TZP based composites have received much attention due to excellent mechanical properties. Strengths of up to 2.5 GPa and fracture toughness' of up to 17 $MPa \cdot m^{0.5}$ have been obtained for the Y-TZP containing 20 % alumina [2]. The addition of micron-sized WC particles to a Y-TZP matrix was reported to increase the hardness significantly [3]. Such excellent mechanical properties are connected with transformation toughening on one hand [4] and with additional toughening mechanisms incorporated by second phase inclusions on the other hand. The major toughening mechanisms in the Y-TZP/WC composites were identified to be microcracking, crack bridging, crack deflection and crack branching [5].

Establishing the crystal relationships between adjacent grains can provide insight into the nature of toughening. So, the second aim of this paper is to describe a pioneering attempt to determine these relationships

in selected zirconia and alumina based composites by using a new technique known as electron backscatter diffraction (EBSD).

2. Processing and properties of Y-TZP/Al_2O_3 Composites

2.1. Processing

Owing to the need to prepare a homogeneous dispersion of the Al_2O_3 reinforcement in Y-TZP and to establish cost-effective processing routs, different methods such as conventional powder processing and wet-chemical processing [6,7] have been developed. The former route involves physical mixing the reinforcement and matrix particles The latter route includes the co-precipitation processing among other techniques (e.g.: mixing a hydrous zirconia/yttria gel with a solution of aluminium acetonate in ethanol and calcination of the dried gel, spraying a suspension of yttria-stabilized zirconia in a dilute solution of aluminium chloride and calcination of the dried gel, enclosing a fine grained α-alumina in a hydrous zirconia/yttria gel structure during co-precipitation and calcination of the dried gel).

Two ways of Al_2O_3 particles incorporation to the 3 mol% Y_2O_3-ZrO_2 powder composed of nanocrystallites will be described in detail: (i) the conventional method of physical mixing α-Al_2O_3 powder with yttria/zirconia one, (ii) the co-precipitation method followed by calcination of deposits, which contained all necessary cations to build zirconia and alumina phase.

2.1.1 Conventional powder route

Generally, conventional powder processing for composites and nanocomposites can be divided into four main steps: (1) selection of the starting powders, (2) wet mixing of the powders, (3) drying the slurries and (4) consolidation.

2.1.1.1 Starting powders

The most important requirements for the starting powders are small particle size, narrow particle size distribution and high purity. Only ultrafine powders for both the matrix and the reinforcement can guarantee satisfactory dispersion of the submicronic or nano-phase in the final product. High purity powders are necessary to avoid the formation of a second phase during sintering. Usually some pre-processing of the reinforcement and matrix powders is needed to remove strength-limiting particle impurities, to deagglomerate and to sort desired size fraction. Careful control over the composite powder morphology helps to avoid increased porosity of the composite due to falling powder sinterability when particles of a second phase are introduced to the system.

Guided by the forgoing criteria, the 3 mol% Y_2O_3 stabilized zirconia powder of a specific surface area of 11.7 m^2/g (CEREL Boguchwała) and the α-Al_2O_3 one of a specific surface area of 4.5 m^2/g with no MgO (NABALOX No 625-31MF) were selected. A choice of the zirconia powder was also subordinated to keeping a particle size comparable with that of the co-precipitated powder. The powders were wet milled by attrition for 2 h using zirconia ball mills of 2 mm in diameter and their resultant characteristics are shown in Table 1.

Table 1. Basic characteristics of the zirconia and α-alumina powder after 2h of wet-attrition milling

Powder	Specific surface area, S_w, m^2/g	Equivalent particle size, d_{BET}, nm	Monoclinic phase content, V_m, %	Crystallite size, nm		
				Monoclinic zirconia, $D_{(111)}$,	Tetragonal zirconia $D_{(11-1)}$,	Alumina, $D_{(110)}$,
3Y-ZrO_2	14.8±0,6	66±3	73	26	36	-
Al_2O_3	7.4±0,4	203±10	-	-	-	124

*± denotes the confidence interval at confidence level of 0.95 in the entire work

The zirconia powder was composed of crystallites having the tetragonal and monoclinic symmetry and a size of 22 nm and 36 nm, respectively. The α-Al_2O_3 powder contained particles of 124 nm in size. The equivalent particle size, d_{BET}, calculated both for the zirconia and alumina powder was larger than the respective crystallite size measured by the X-ray diffraction method. This indicates the presence of agglomerates and/or aggregates in those powders. TEM observations revealed the agglomerate structure of the powders.

2.1.1.2 Powder mixing

Conditions for uniformity of the mixture in a scale of individual particles have to be satisfied. When mixing two different constituents in a suspension, it is necessary to control their surface chemistry via the charged double layer. Dispersed or flocced powders can be used depending on a formation method applied.

The homogenisation of the powder mixtures can be achieved by either wet ball milling or attritor milling techniques in both organic or aqueous media.

In this study, the zirconia powder was mixed with the α-Al_2O_3 one by using attrition milling with zirconia ball mills of 2 mm in diameter for

2 h in the water environment. The pH value was adjusted to 7.5 during mixing to produce a heteroflocculation effect in which the zirconia and alumina particles had an opposite sign of the surface charge (a zeta potential value of –21.1 ± 4.0 mV and 15.4 ± 4.1 mV was measured for zirconia and alumina particles, respectively). Therefore, the particles of the same phase repeal each another whilst those of different phases attract one another. This is conductive in achieving uniformity of the system after drying.

A series of the conventionally prepared powders is called P.

2.1.2 Co-precipitation processing

Alternatively to the conventional processing, the composite powders can be prepared by means of wet-chemical methods. These special methods enable not only to join preparation of both constituents in one process and to control purity of the system precisely but also to obtain the powders that contain nanoparticles. So, nanocomposites containing the reinforcement particles ≤ 100 nm can be produced using such powders.

Co-precipitation of solids from a supersaturated solution is one the most frequently used method for preparation of the zirconia and zirconia based powders. This process is attractive due to its simplicity, versatility and availability of law cost precursors. Inorganic salt compounds used in the co-precipitation method are more versatile and economical than alkoxides employed in the sol-gel process, which is also utilized in the zirconia containing systems.

To prepare the alumina/zirconia composite powder, aluminium nitrite ($Al(NO_3)_3 \cdot 9H_2O$; analytically pure) and zirconium oxychloride

($ZrOCl_2 \cdot 8H_2O$; pure) were dissolved in distilled water and yttrium oxide (Y_2O_3; 99.99%) in hydrochloric acid. The three solutions were blended in the suitable proportion and the resultant one was introduced to a vigorously stirred ammonia solution (3.55 M). A pH value was kept of 8.5 at the end of the process. The deposits were washed with ammonia solution (pH=8.5), dried and then calcined for 2 h at 1100°C. The powders were milled in an attritor using zirconia ball mills of 2 mm in diameter and the water environment. The milling time enabled a specific surface area of the resultant powder of ~15 $m^2 \cdot g^{-1}$ to be obtained. A series of the co-precipitation processed powders is called C.

Table 2. Basic characteristics of the C series powders.

Al_2O_3 content, vol.%	Specific surface area, S_w, m^2/g		Milling time, t, h	Equivalent particle size, d_{BET}, nm	Monoclinic phase content, V_m, %	Crystallite size, nm		
	As-calcined powders	Milled powders				Monoclinic zirconia, $D_{(111)}$	Tetragonal zirconia $D_{(11\text{-}1)}$	Alumina, $D_{(113)}$
0	9.0	15.1	2	65	48	32	30	-
0.5	8.4	13.2	2	75	-	-	-	-
1.0	9.6	14.0	2	71	-	-	-	-
2.5	8.8	15.3	3.5	65	-	-	-	-
5.0	9.1	15.7	2	64	23	29	16	-
10.0	4.4	12.5	5.5	82	29	17	10	-
20.0	23.8	30.8	2	34	39	15	11	91

The C series powders contained tetragonal and monoclinic crystallites of zirconia solid solution and α-Al_2O_3 (Table 2). The monoclinic phase content in a zirconia part of the composite powder was statistically independent on milling time and alumina content but a size of zirconia crystallites decreased with alumina content. This was

accompanied by an increase in the specific surface area of the *C20* powder over a value of 15 m^2/g. The similar influence of alumina on zirconia crystallite size and specific surface area of the zirconia/alumina co-precipitated powders was reported in Ref. [6-8]. The C series powders were agglomerated as indicated by larger values of d_{BET} then those of D_t and D_j and TEM observations. The α-Al_2O_3 crystallites had the size of ~91 nm (*C20*).

2.1.3 Consolidation

Although expensive, hot-pressing has predominantly used for the consolidation of composites containing both submicronic and nanometric particles. Generally, hot pressing is carried out using a graphite die, with pressures between 20 and 40 MPa, and temperatures between 1500 and 1800°C, all under Ar or N_2 atmosphere.

Cold pressing, slip casting, injection moulding and pressure filtration have all been used to produce green compacts with densities as high as possible (up to 62%) for pressureless sintering [9].

For comparison, both consolidation methods were used to produce the Y-TZP/alumina composites under study. Samples for pressureless sintering were shaped by cold-isostatic pressing under 300 MPa. Oleic emulsion in amount of 5 % was added to the powders as lubricant. The green compacts were pressureless sintered for 2 h at the temperatures ranging from 1500 to 1650°C. A heating rate of 2°C/min below 450°C and 5°C/min above this temperature was used. Hot pressing of the powders was performed under 25 MPa in argon for 2 h at 1500°C using the heating cycle the same as in the case of pressureless sintering.

2.2 Particle packing within green bodies

There are a large number of critical processing parameters for pressureless sintering. Most important is the preparation of the green compacts from which density and uniformity of particle packing depends.

The P series powders showed better compressibility than those of the C series as illustrated in Fig. 1. Additive of the big corundum particles

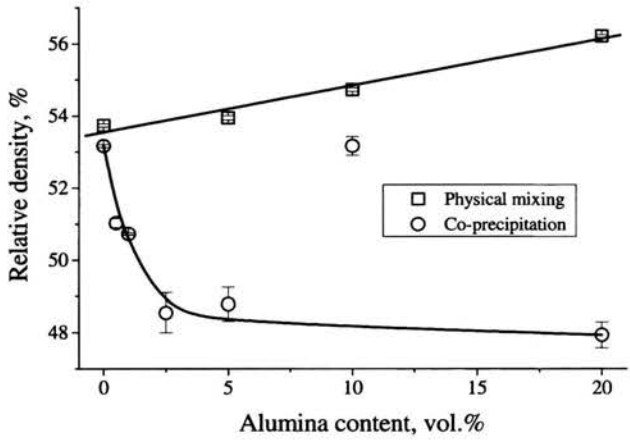

Fig. 1. Relative density of green compacts shaped under 300 MPa vs. Al_2O_3 content

increased linearly density of the compacts (correlation coefficient R=0,989 at probability P=0,011) according to the rule of mixture. Mercury porosimetry measurements revealed monomodal pore size distributions in the compacts derived from the powders both of the C and F series (Fig.2). The pore size distributions in case of the P compacts were practically independent on the content of alumina particles (d_{50}=0.057±0.003 μm). More significant influence of alumina content on

the pore size distribution was observed in the case of the C compacts. Except for the C0, C10 and C20 compacts, the other ones studied contained the pores of very similar size (d_{50}=0.058±0.002 μm) comparable with that of the P compacts.

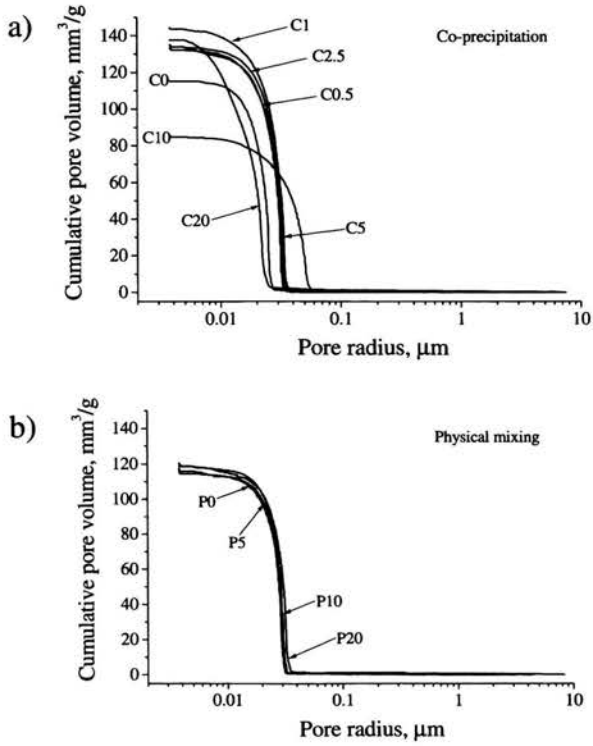

Fig. 2. Pore size distributions of compacts: a) C series, b) P series. Indicated is Al_2O_3 content

2.3 Density and microstructure of the sintered bodies

The final densities of composites fabricated by pressureless sintering are usually somewhat lower compared to materials densified by hot-pressing

as confirmed by data of Fig. 3. This figure illustrates also an effect of the powder processing method on densification of the sintered materials. Common tendencies observed are as follows: (i.) a decrease of densities accompanied by the temperature increase above 1500°C, (ii.) the lack of significant effect of the Al_2O_3 content on densification of the materials. An increase of the sintering temperature more disadvantageously influenced densification of the co-precipitated powders with alumina content <5 vol.% than those physically mixed (Fig. 3a). The materials derived from the C series powders showed also larger variations of densities among successive points of alumina content. In case of the *C10* samples such behaviour can be attributed to the pore size distribution in the green compact shifted towards

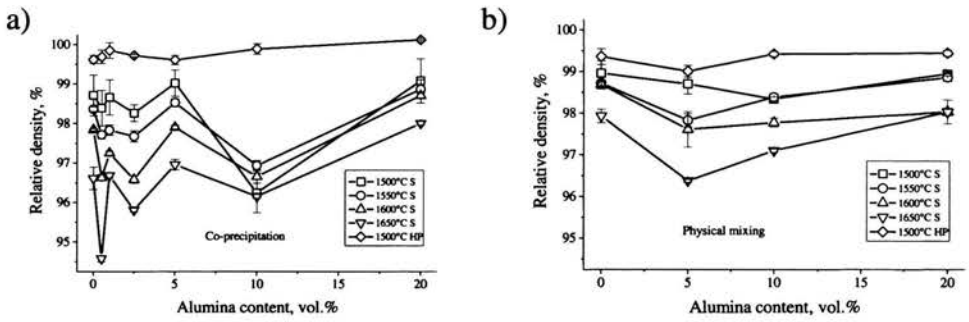

Fig. 3. Relative density of sintered materials vs. Al_2O_3 content: a) C series, b) P series; S – pressureless sintering; HP – hot pressing. Indicated is the sintering temperature

bigger pores (Fig. 2a) but in case of other samples it should be attributed to non-uniformities of particle packing within the compacts not detected by mercury porosimetry. Hot pressing under 25 MPa removed effects of morphological imperfections of the powders to a very large extent. After

sintering at 1500°C, the hot-pressed bodies reached nearly theoretical densities of 99.8±0.2 and 99.3±0.3% for the series C and P, respectively.

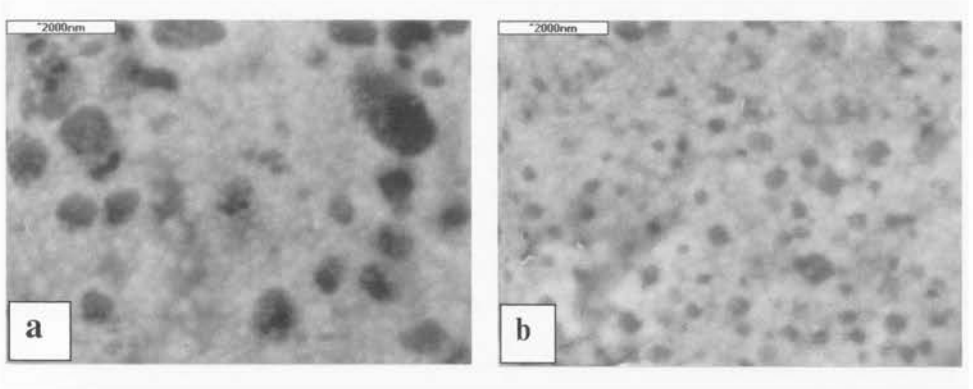

Fig. 4. SEM micrographs of the TZP/Al_2O_3 composites containing 20 vol.% of alumina produced by means of a) physical mixing, b) co-precipitation. The sintering temperature was 1500 °C

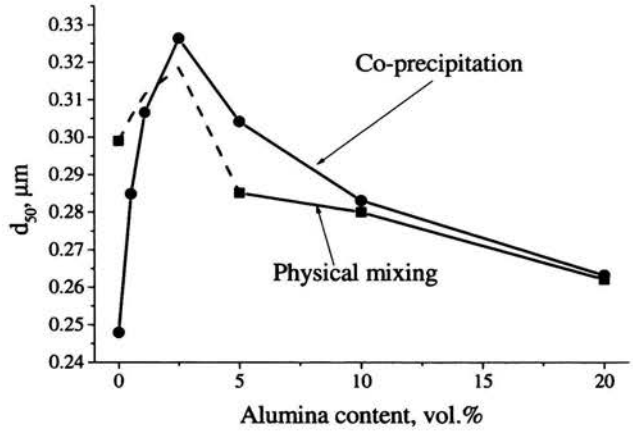

Fig. 5. Median zirconia grain size, d_{50}, vs. alumina content in the composites. Indicated is the preparation method

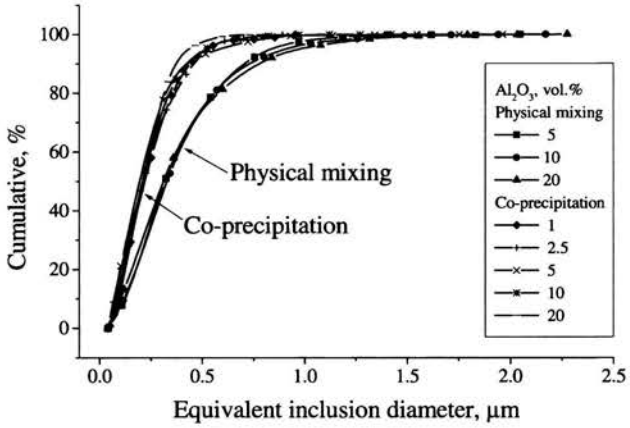

Fig. 6. Distributions of the alumina inclusion size in the TZP/Al_2O_3 composites. Indicated is the preparation method and alumina content

SEM observations revealed homogeneous dispersion of the alumina inclusions within uniform zirconia matrix for both P and C series (examples shown in Fig.4). The data of Figs 5 and 6 indicate that, when the size of zirconia grains remains on the comparable level, the co-precipitation method is suitable for the preparation of TZP/Al_2O_3 composites with alumina inclusions of a size much smaller than that originated from physical mixing. The former one comes into the nanometric range. For both series, the size of alumina inclusions was practically independent on their content in the range studied. A mean median value of alumina inclusions was 0.32±0.2μm and 0.21±0.01μm for the P and C composite series, respectively. A width of the inclusion size distribution was narrower for the latter one.

Quantitative measurements of zirconia grain size distributions indicated that the alumina particles inhibited zirconia grain growth (Fig 5) for the alumina contents larger than 2.5 vol.%. The Al_2O_3 addition in the range of 0.5-2.5 vol.% produced zirconia grain growth in the

composites of the C series. This could originate from the possible formation of liquid phase in the reaction of silica with alumina and yttria and therefore the occurrence of liquid phase sintering. Silica is a typical impurity of zirconia salts. The eutectic mixture composed of 45% SiO_2, 20% Al_2O_3 and 35% Y_2O_3 is reported in the SiO_2-Al_2O_3-Y_2O_3 system at the temperatures 1300-1400°C [10]. The analogous effect is anticipated in the P series composites (dashed line in Fig. 5).

2.4 Mechanical properties

The X-ray diffraction analysis of phase composition of the sintered bodies revealed a zirconia solid solution of tetragonal symmetry in the 3Y-TZP materials (C0 and P0) and additionally α-Al_2O_3 in the composites. Zirconia solid solution of cubic symmetry has been also found in amount of 9.9±0.1 wt% and 8.7±0.2 wt% in the materials of the C and P series, respectively; the rest was tetragonal zirconia

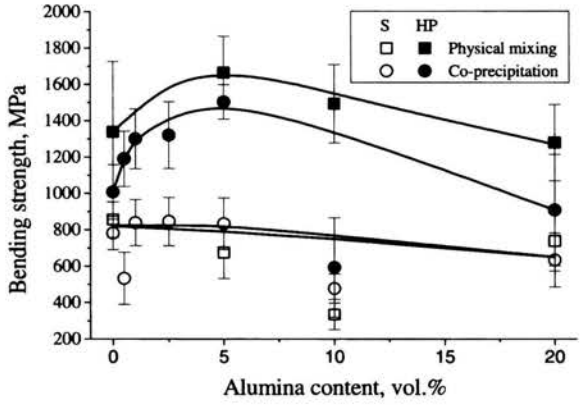

Fig. 7. Bending strength of the pressureless sintered (S) and hot-pressed (HP) bodies at 1500°C vs. Al_2O_3 content. Indicated is the powder preparation method

The results of the three point bending test of the samples sintered at 1500°C are shown in Fig.7. The reinforcement effect due to the alumina incorporation has not been found in the TZP's pressureless sintered. A falling tendency of fracture strength with alumina was observed for both series of composites studied. A statistical analysis (t test) indicated that difference between the mean values of fracture strength of the C and P composites with the same alumina content is essential at probability level of 0.05 only in the case of the samples that contained 5 and 10 vol.% of alumina. Hot pressing raised fracture strength within the range of 25 % (*C10*) – 350 % (*P10*). A mean increase of strength due to hot pressing was higher for the P series of materials (156%) than that for the C one (59 %). The reinforcement effect due to the alumina incorporation was clear in the hot pressed composites. The highest fracture strength of 1.7±0.2 GPa has been measured for the TZP contained 5 vol.% of alumina particles.

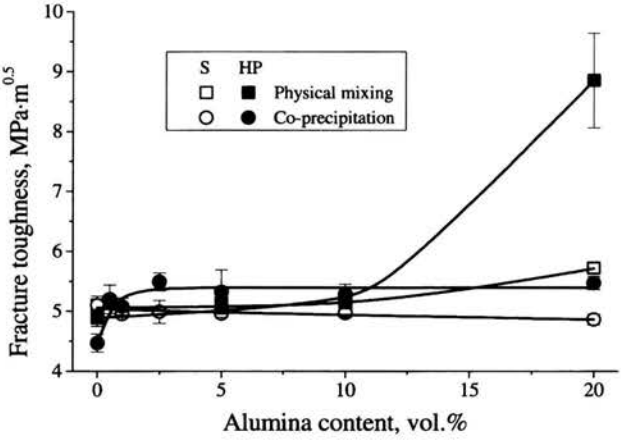

Fig. 8. Fracture toughness of the pressureless sintered (S) and hot-pressed (HP) bodies at 1500°C vs. Al_2O_3 content. Indicated is the powder preparation method

The relationship between alumina content and fracture toughness of the C and P series of materials is shown in Fig. 8. With the exception of the TZP composite, which contained 20 vol.% alumina, other materials showed moderate values of fracture toughness. They changed from 4.5±0.1 $MPa \cdot m^{0.5}$ to 5.7±0.1 $MPa \cdot m^{0.5}$. Fracture toughness was only slightly affected by the alumina content, method of alumina incorporation and consolidation method.

The data collected above illustrate the relation between the properties, processing and microstructure of ceramics. Both physical and chemical method of incorporation of alumina particles into the mixture with tetragonal ones affected morphological features of the powders such as a size of crystallites, primary particles and agglomerates. The powder morphology together with agglomerate strength influences particle packing within green bodies and further a microstructure of the consolidated materials i.e. grain size both of the matrix and inclusions, uniformity of their dispersion, content and size of pores. The last two features depend on consolidation method applied in decisive manner. According to the Griffith's theory [11], fracture strength is proportional to the critical stress intensity factor and it is inversely proportional to the square root of the critical flaw length. Because fracture toughness of the TZP/Al_2O_3 composites studied was practically independent on the consolidation method applied, the increase of fracture strength observed in the case of hot-pressed materials should be attributed to a reduced size of pores that are the main stress concentrators. The same reason was responsible for the lower fracture strength of the hot-pressed composites

of the C series when compared to the P one. The microstructure image analysis confirmed the pore size reduction (Table 3). Additionally, it revealed a decrease of defect density (defined as a number of pores in 10^4 μm^2) in the hot-pressed samples. The data of Table 3 illustrate a rule that small changes in relative density of nearly fully densified materials cause great changes in their porosity.

The above interpretation is consistent with observations of many researchers who studied the influence of consolidation method on mechanical properties of zirconia based composites and ceramics generally. Lange [12] reported that the hot isostatic pressing improved the fracture strength of the composite materials in theY_2O_3-PSZ/Al_2O_3 system. He pointed out that defects introduced by the fabrication process were responsible for the decrease in fracture strength of both pressureless sintered and isostatically hot-pressed materials. Tsukuma [2] and Fukuhara [13] reported the same behaviour. They have found that pressureless sintered TZP/Al_2O_3 composites showed a fracture strength of ≈1 GPa but of >2 GPa after additional hot isostatic pressing.

It is worth to notice that the reduction of alumina inclusion size to a close nanometric one did not lead to the increased values of fracture strength and fracture toughness of the TZP/Al_2O_3 composites. This suggests that in the case of nanocomposites with intergranular inclusions a spectacular increase of mechanical properties should not be expected, especially when the composites are not fully densified. Sternitzke [9] came to the same conclusion in the case of Al_2O_3/SiC and Si_3N_4/SiC nanocomposites.

He stated that the strength increase can best be related to a reduction in processing defect size.

Table 3. Porosity characteristics of the chosen materials that were pressureless sintered and hot-pressed (P=25 MPa) using the same heating cycle

Material	Relative density, %	Porosity, vol. %	Maximum pore size, μm	Number of pores in 10^4 μm^2
Pressureless sintering				
P0	98.96±0.30	1.04	2.7±0.5	82±24
P5	98.70±0.24	1.30	3.3±1.8	66±20
P100	96.87±0.04	3.13	7.4±2.1	201±24
Hot-pressing				
P0	99.36±0.19	0.64	1.4±0.6	6±4
P5	99.01±0.14	0.99	1.1±0.3	6±4
P100	99.64±0.14	0.36	2.6±0.5	60±18

3. TEM and EBSD studies of crystal orientations in Al_2O_3/WC composites and Y-TZP reinforced with WC, NbC and TaC particulates

Microstructure of ceramic composites can be better understood by establishing crystallographic relationships between adjacent grains. Such determination can be successfully performed by transmission electron microscopy (TEM). Thin foil examination reveals information on adherence of grains, the presence of cracks and voids and, what is the most important, on the crystallographic relationships between the matrix and reinforcing grains by examination of selected area electron diffraction (SAED) patterns.

However, during TEM experiments, the observed area is limited to few grains only. Thus, it is difficult to collect statistically reasonable

amount of data. Moreover, the preparation of thin foils from ceramic composites composed of phases of different hardness is arduous and time-consuming. A technique known as the EBSD (Electron Back Scatter Diffraction or Orientation Imaging Microscopy in the Scanning Electron Microscope (OIM/SEM)) [14-16] has been employed to overcome such problems. It provides a wealth of information about the orientation of crystals with spatial resolution in the range of a few tenths of micrometer, depending on the beam accelerating voltage, specimen tilt and probe size as well as specimen density. Recent developments in data processing have also improved significantly angular resolution up to 0.5°. A relatively large number of diffraction patterns from several hundred of neighbouring grains can be collected, indexed and stored during one single experiment by applying the EBSD technique. Consequently, orientation relationships between several or even hundreds of grains can be established giving a sufficient ground for general characteristics of the material.

3.1 Processing and selected properties of Al_2O_3 and Y-TZP reinforced with carbide particulates

Conventional powder processing was used to prepare composites in the Al_2O_3/WC, Y-TZP/WC, Y-TZP/NbC and Y-TZP/TaC systems for TEM and EBSD studies. The commercial α-alumina, zirconia stabilized with 2.9 mol % of yttria, WC, TaC and NbC powders were used. Each carbide powder was ground in a rotation-vibration mill to reduce a particle size. The composite powder was homogenized by attrition

milling in ethyl alcohol. Hot-pressing under 25 MPa or pressureless sintering, all in argon, has been used for the consolidation of the composites. Sintering temperatures and selected properties of the composites are shown on Table 4.

Table 4. Properties of the Y-TZP, alumina and the composites with selected carbides

Material	Consolidation conditions	Density, % theo.	Young modulus, E, GPa	Vickers hardness, HV, GPa	Fracture toughness, K_{Ic}, $MPa \cdot m^{0.5}$
Y-TZP	1500 PS	99.0±0.1	221 ±2	14.4 ±0.5	6.0 ±0.1
	1400 HP	99.7±0.1	209 ±3	14.1 ±0.3	4.6 ±0.2
Y-TZP/10% WC	1500 PS	98.8±0.1	238 ±3	17.0 ±1.5	6.7 ±0.8
	1400 HP	98.8±0.1	232 ±2	19.0 ±0.6	9.7 ±1.0
Y-TZP/20% WC	1500 PS	96.2±0.1	259 ±3	16.8 ±0.6	7.3 ±1.3
	1400 HP	98.9±0.1	265 ±4	21.0 ±0.6	7.0 ±0.5
Y-TZP/20% NbC	1500 PS	99.2±0.1	216 ±4	15.4 ±1.3	5.8 ±0.6
Y-TZP/20% TaC	1500 HP	99.8±0.1	231 ±5	17.0 ±0.9	5.3 ±0.4
Al_2O_3	1700 HP	99.0±0.1	380±5	15.0±1.2	4.5±0.5
Al_2O_3/10vol.% WC	1700 HP	98.5±0.1	430±3	17.0±1.5	6.0±0.6

PS – pressureless sintering, HP – hot-pressing

The incorporation of carbide particulates into both the TZP and alumina matrix results in increase of mechanical properties which depends on a kind of carbide, its content and processing conditions as shown in Table 3.

3.2 Sample preparation for TEM and EBSD measurements

Specimens for TEM observations were prepared by cutting 3 mm diameter discs and polishing them to a thickness of 30 to 40 μm. Then the sample was dimpled (GATAN Dimple Grinder) up a thickness of less

than 10 μm and finally thinned by ion milling (GATAN Duo Mill) applying argon ion guns at different angles (from 10° up to 20°). Thin foil was examined at 200 kV.

Sample surfaces designed for the EBSD measurements should be flat and free of stresses. Surface undulations cause local variations in surface normal directions about the bulk tilt angle. The tilt variations deteriorate Kikuchi band contrast and, consequently, reduce the number of Kikuchi patterns suitable for indexation. Further, the EBSD measurements require the size of grains above the resolution of the method. For typical resolution of 200 nm (or better) obtained in the SEM with W filament, the grain size should be above 1 μm to get reasonably good statistics.

The effect of preparation conditions on surface topography will be discussed on the example of Y-TZP/WC composite.

In order to eliminate any distortion in a subsurface layer which might have appeared during the sample preparation for EBSD measurements the composite must be treated with extreme caution. Conductive thermoplastic resign was used for mounting. Then, the sample was polished with diamond pastes of decreasing grain size and, finally, by colloidal silica under lowpressure (20-30 N) to minimize surface mechanical damage since Bragg diffraction of electrons occurs below 50 nm of the specimen surface [17].

Additional heat treatment, which removes the polishing-induced stresses, was performed for 40 minutes at 1350°C in an argon atmosphere to prevent oxidation of the carbide phase. in order to. A very thin carbon

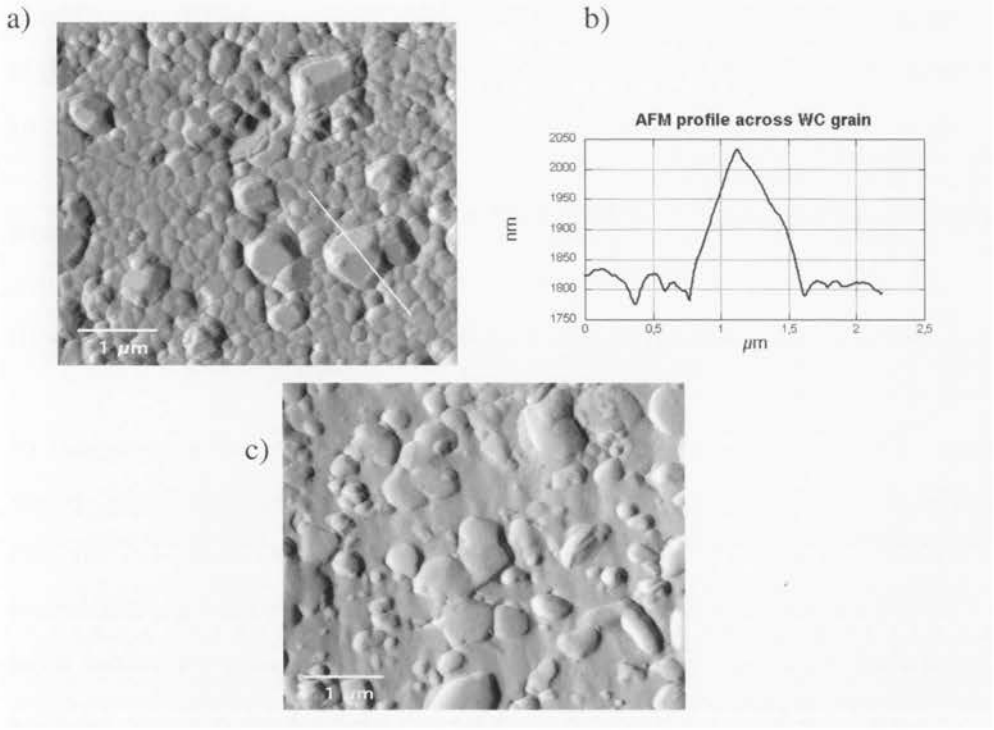

Fig. 9: Atomic Force Microscopy results (Topometrix Explorer 2000 AFM, contact mode): a) image obtained from the thermally etched Y-TZP/WC composite. Small Y-TZP grains surround facetted WC particles protruding from the matrix; b) topographic profile across a WC grain (line scan is shown in Fig. 9a); c) image obtained from the Y-TZP/WC composite polished with colloidal silica

coating was deposited on each sample, since charging of uncoated composites made impossible acquisition of the Kikuchi patterns.

The surface topography of the heat treated after sample is shown in Fig. 9a. The WC particles (some of them are facetted) protrude from the matrix up to 200 nm height (Fig. 9b) due to differences in wear resistance of the carbide and oxide phase ($E_{carbide}$= 14 GPa and E_{oxide} = 19 GPa). The sample, which was only polished with colloidal silica (Fig. 9c),

exhibits less distinctive surface topography, however, due to the different wear resistance of WC and zirconia grains, some differences in height still exist. Optimisation of the polishing and thermal etching conditions can reduce this effect.

Sample charging inhibits the collection of Kikuchi patterns considerably. Deposition of a very thin carbon coating eliminates this problem to some extend. Restricting the sample size to approximately 10 mm x 10 mm or less also mitigates charging.

Despite these problems, EBSD data from relatively large regions of the Y-TZP based composites can be obtained. In such case, phase orientation maps reveal the distribution of composite phases, i.e. zirconia modifications and reinforcement, and some regions, where the diffraction patterns could not be analysed are also present. This is connected most probably with both the sample roughness and a size of some zirconia matrix grains which is below the system resolution.

3.3 Measurement and equipment

To perform electron backscatter diffraction analysis separate match units for tetragonal and monoclinic zirconia, Al_2O_3, WC, NbC and TaC had to be created. The match unit contains reference crystal data and lists of Kikuchi bands for each phase. The precise crystallographic data recorded by the X-ray diffraction (XRD) had to be evaluated. The values that were used for match unit creation are listed in Table 5.

Table 5. Crystallographic data for creation of the match units

Phase	Symmetry	Laue group symmetry	Cell parameters			
			a, Å	b, Å	c, Å	β,°
ZrO_2	tetragonal	4/mmm	5.1023		5.1817	
ZrO_2	monoclinic	–2/m	5.1460	5.212	5.313	99.2
Al_2O_3	trigonal	-3m	4.758		12.991	
WC	hexagonal	6/mmm	2.9046		2.8356	
NbC	cubic	m3m	4.4693			
TaC	cubic	m3m	4.4529			

In the case of alumina/WC composites the SEM and EBSD measurements were carried out in a LEO 438 VP scanning electron microscope with hairpin tungsten gun at the acceleration voltage 20 kV, tilt angle 70° and working distance 25 mm in a variable pressure mode to neutralize a negative charge gathered under the surface of composite. Carbon coating appeared to be less desirable method to eliminate charging effects as it deteriorates Kikuchi bands quality significantly leading to decrease of number of solved patterns. The backscatter diffractions were acquired and indexed by the TSL TexSEM hardware. Then, all collected data were transformed into the HKL Technology format and analysed by use of two CHANNEL 5 programmes, mainly *Tango* for generating a wide variety of maps, e.g. orientation, and measuring grains, and *Mambo* for producing pole figures and inverse pole figure from EBSD orientation data. Grid resolutions of 0.25 μm and 0.2 μm were chosen to reveal fine microstructure details.

In the case of zirconia based composites the measurements were carried out in a PHILIPS XL30 scanning electron microscope with field emission gun (FEGSEM) at the acceleration voltage 20 kV, tilt angle 70°

and working distance 16 mm. The backscatter image was analysed and indexed with NORDIF EBSD hardware and CHANNEL+EBSD software for fully automated pattern indexing. A grid resolution of 0.05 μm was chosen to reveal small microstructural details and their orientation properties.

3.4 Microbeam Studies of Alumina-WC Composites

Measurements performed in the TEM revealed the matrix and tungsten carbide grains close adhering and any discontinuities. A thin, glassy, amorphous phase was detected in sizeable pockets observed at triple points. Alumina and WC grains were indexed using the SAED and two characteristic crystal relationships between above phases were identified (Figs 10 and 11):

$$(0\,1\,1\,1)\ WC \parallel (1\,1\,0\,5)\ Al_2O_3$$

$$[1\,1\,2\,3]\ WC \parallel [2\,3\,1\,1]\ Al_2O_3$$

and

$$(0\,1\,1\,1)\ WC \parallel (1\,0\,1\,1)\ Al_2O_3$$

$$[2\,1\,1\,0]\ WC \parallel [0\,1\,1\,1]\ Al_2O_3$$

A confirmation of these crystal correlations in a much larger volume has been found by using the EBSD. Single orientation measurements were recorded and displayed in a form of phase orientation maps (Figs 12 and 13). Stereographic projections of particular crystal directions in the alumina and tungsten carbide phases within the sample surface plane were calculated from the analysis of subsets which enabled to select areas where neighbouring grains of two different phases stick to each other.

The data of Figs 12 and 13 indicate that in the adjacent alumina and tungsten carbide grains certain crystal planes, mainly: (1 1 $\bar{0}$ 5) in Al_2O_3 and (0 1 $\bar{1}$ 1) in WC as well as directions <0 1 $\bar{1}$ 1> in Al_2O_3 and <2 $\bar{1}$ 1 0> in WC are nearly parallel. These results confirm previous SAED measurements performed in the TEM, however in a much greater scale.

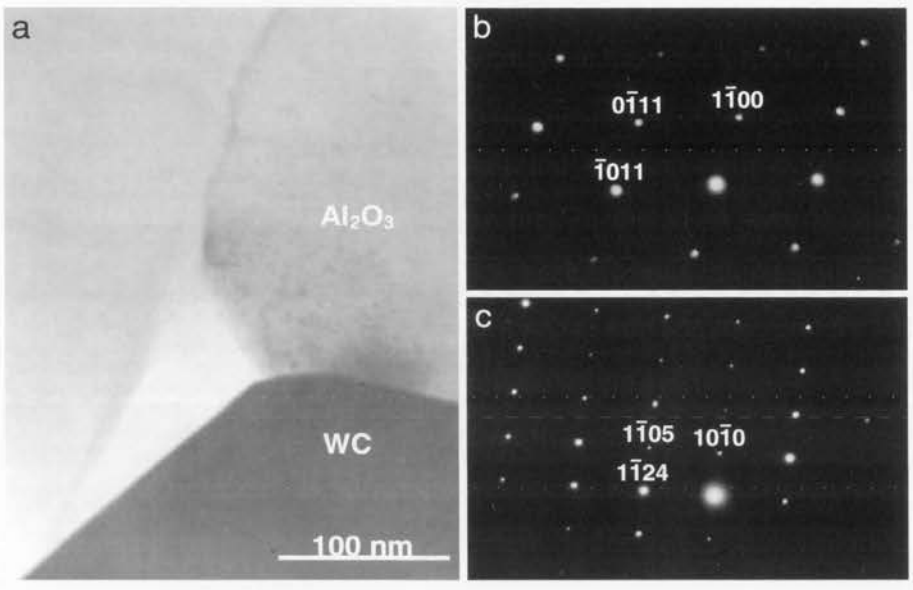

Fig. 10: TEM micrograph of Al_2O_3, a) BF, b) SAED from WC, c) SAED from Al_2O_3

It must be added that in the investigated system the thermal expansion coefficient mismatch (CTE) is not as significant as in the other composites [18]. The values of the CTE for Al_2O_3 and WC ($\alpha_{Al2O3}=7\times10^{-6}°C^{-1}$ and $\alpha_{WC}=5.2\times10^{-6}°C^{-1}$) result in relatively low internal stresses during cooling after sintering. This fact reflects in less diffused Kikuchi bands compared with e.g. the Y-TZP/WC system, in which CTE mismatch-induced tensile stresses are much higher ($\alpha_{Y\text{-}TZP}=11\times10^{-6}°C^{-1}$).

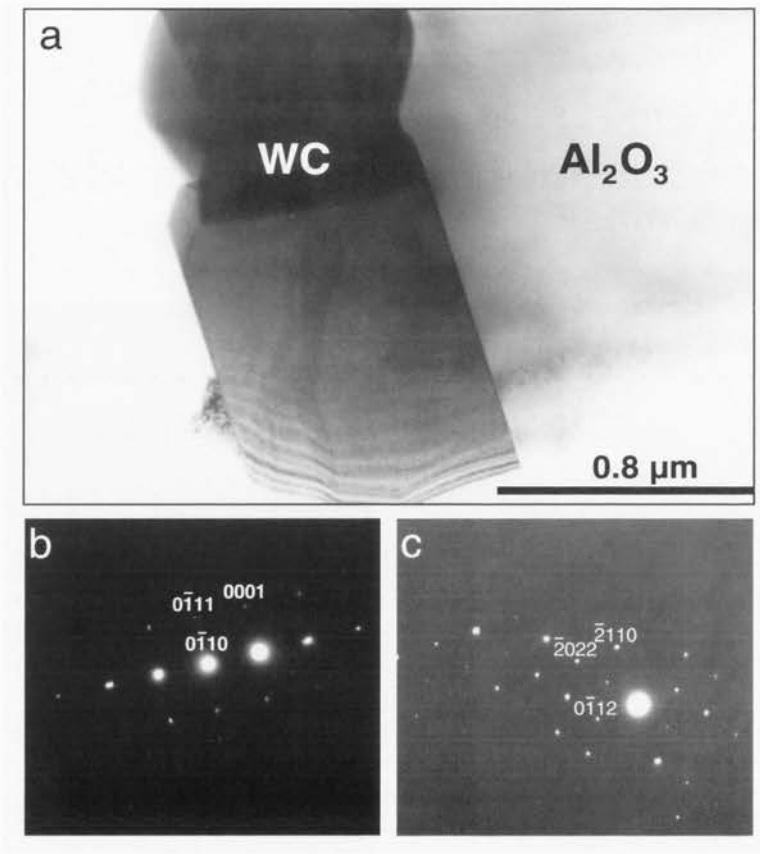

Fig. 11: TEM micrograph of Al_2O_3, a) BF, b) SAED from WC, c) SAED from Al_2O_3

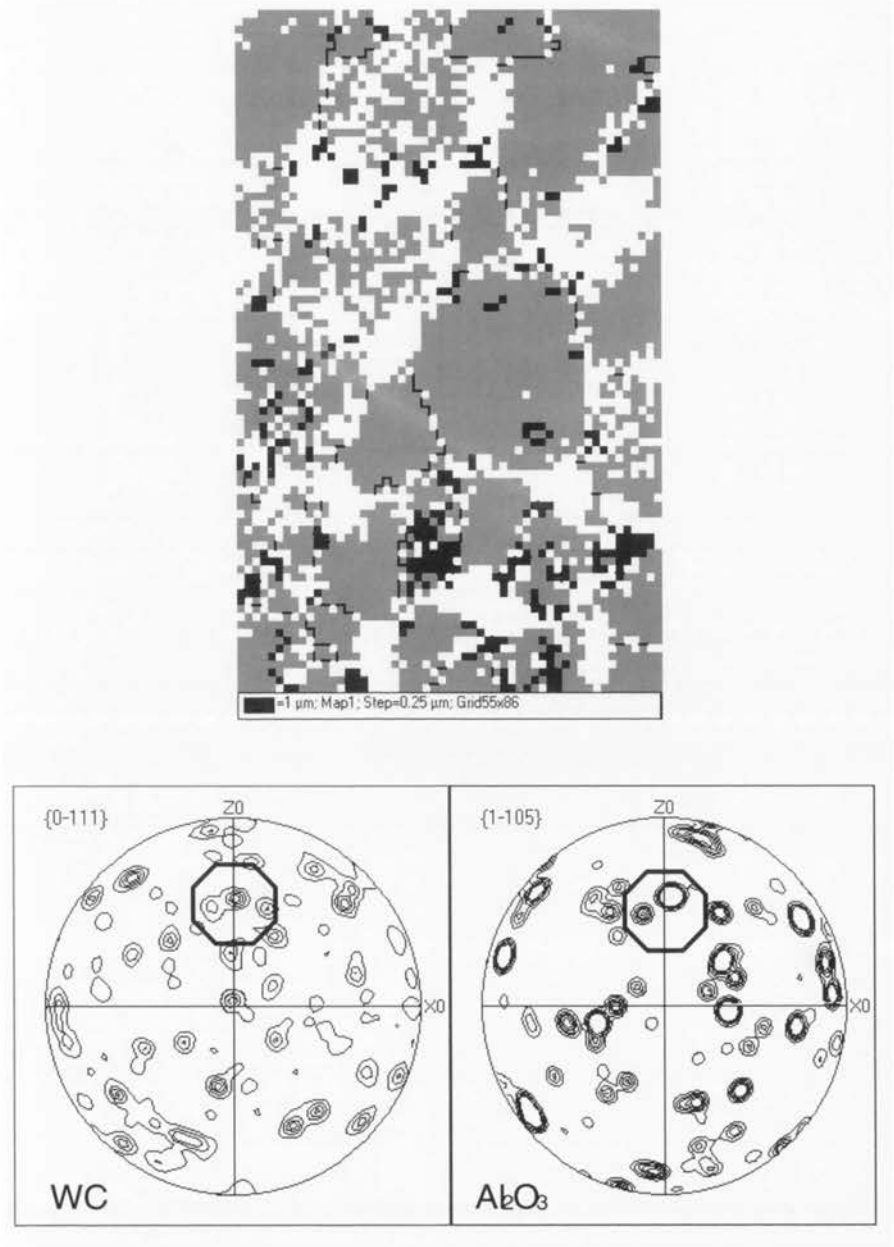

Fig. 12: EBSD orientation map with pole figures (planes) representing crystal relationship from Fig.10; grey and black regions represent Al_2O_3 and WC, respectively; white areas have not produced analysable diffraction pattern

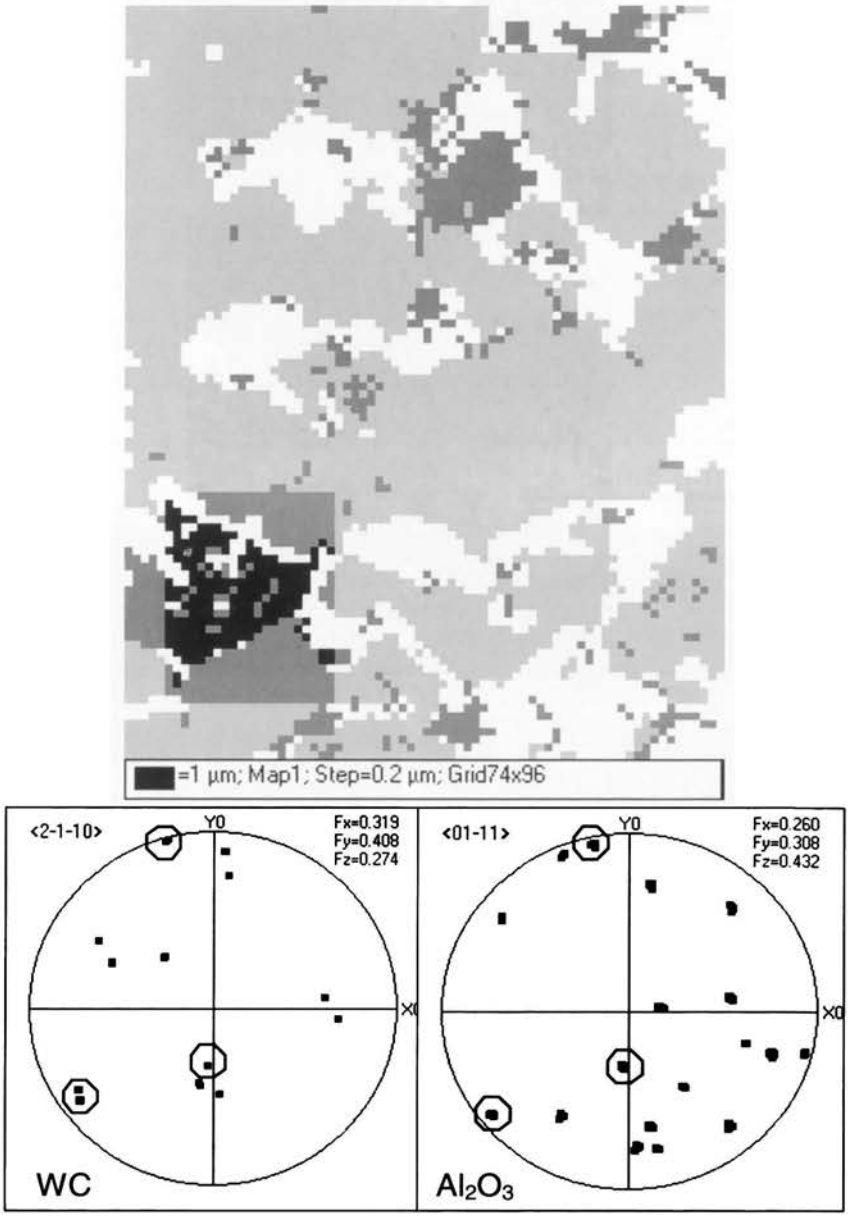

Fig. 13: EBSD orientation map with a marked subset from which pole figures (directions) representing crystal relationship shown in Fig. 11 were calculated; grey and black regions represent Al_2O_3 and WC, respectively; white areas have not produced analysable diffraction pattern

3.5 TEM and EBSD studies of Y-TZP/WC composites

An analysis of Y-TZP and WC grains by means of the selected area electron diffraction method (SAED) gave the following crystal relationships between these phases [18, 19]:

$$[0001]\ \text{WC} \parallel [001]\ \text{t-}ZrO_2$$

$$[\bar{1}\,010]\ \text{WC} \parallel [010]\ \text{t-}ZrO_2$$

A phase orientation map revealed the distribution of the tetragonal and monoclinic zirconia and WC. There were some areas where the diffraction patterns could not be analysed mostly due to the sample roughness and the Y-TZP grain size being below the system resolution. Global distributions of selected crystal directions in the Y-TZP and WC phases indicated on a rather wide spectrum of randomly distributed orientations.

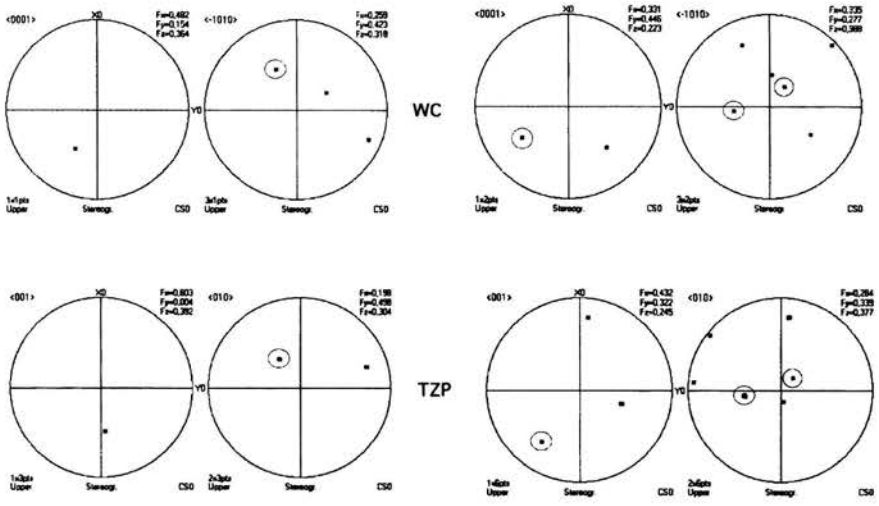

Fig. 14: Crystal directions of neighbouring WC and Y-TZP grains in the selected areas called subset 1 and subset 2 in Fig. 2. Circles mark parallel crystal directions

Stereographic projections of particular crystal directions in the tetragonal zirconia and hexagonal tungsten carbide phases within the sample surface plane were calculated from the analysis of small areas near the phase boundary. Figure 14 shows two typical examples of the crystal directions arrangements in the neighbouring grains of different phases. It can be seen that in the adjacent zirconia and tungsten carbide grains some crystal directions, mainly <001> and <010> in tetragonal zirconia and <0001> and <1010> in tungsten carbide are nearly parallel. These results confirm previous SAED measurements performed in the TEM [18,19].

3.6 Y-TZP/NbC and Y-TZP/TaC composites

Figs 15 and 6 illustrate TEM micrographs of the Y-TZP/NbC and Y-TZP/TaC sample, respectively, with the corresponding diffraction patterns. The diffraction data indicate the following crystallographic relationships between the zirconia matrix and NbC:

$[\bar{1}12]$ NbC ‖ [111] ZrO_2

[110] NbC close to $[\bar{1}10]$ ZrO_2

and between the zirconia matrix and TaC:

[001] TaC ‖ [013] ZrO_2

[100] TaC close to [100] ZrO_2

Several crystal orientation maps acquired by using EBSD enabled to calculate stereographic projections of particular crystal directions in the tetragonal zirconia and carbide phases within the sample surface plane from the analysis of small areas near the interphase boundary.

Fig. 17a shows an example of the stereographic projections of the crystallographic direction [$\bar{1}10$] and [001] of Y-TZP and [100] of the neighbouring TaC grain on the plane of the sample surface. It can be seen that in the adjacent zirconia and TaC grains several crystal directions are nearly parallel. A similar phenomenon has been observed in the Y-TZP/NbC sample. The example of the stereographic projections of the crystallographic directions [010] and [111] of Y-TZP and [110] of adjacent NbC grains on the plane of the sample surface (Fig. 17b) confirms also that in this case several crystallographic directions are almost parallel.

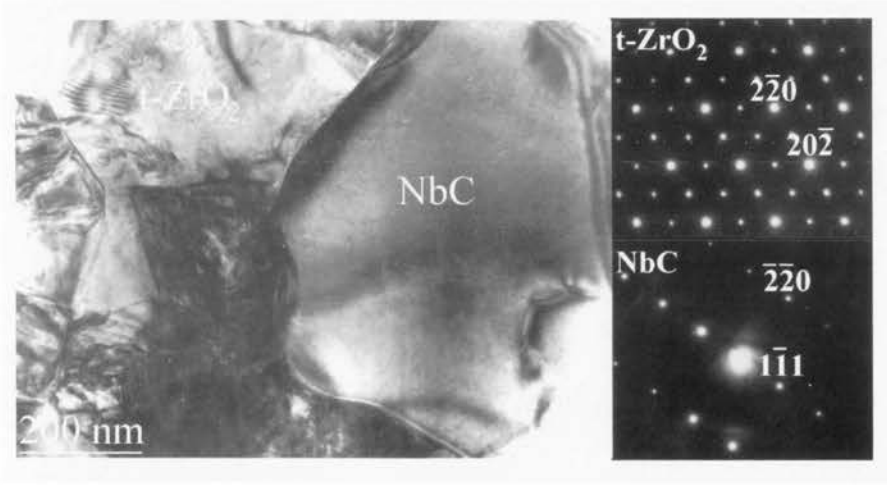

Fig. 15. TEM micrograph of the Y-TZP/NbC composite with corresponding SAEDs taken from Y-TZP and NbC

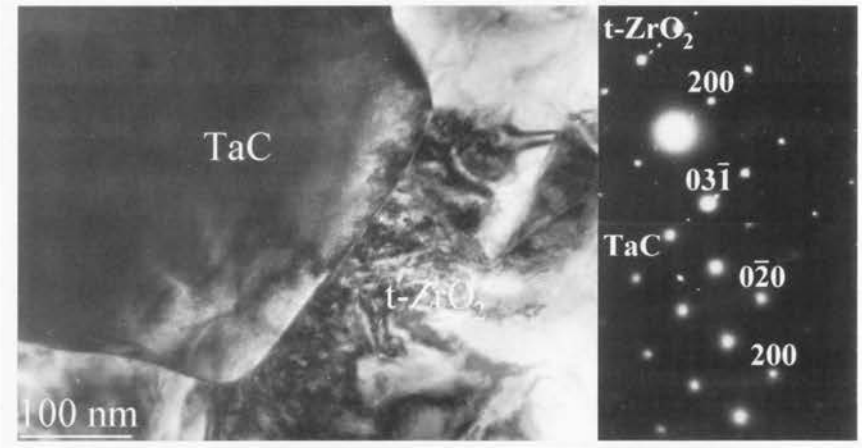

Fig. 16. TEM micrograph of the Y-TZP/TaC composite with corresponding SAEDs taken from Y-TZP and TaC

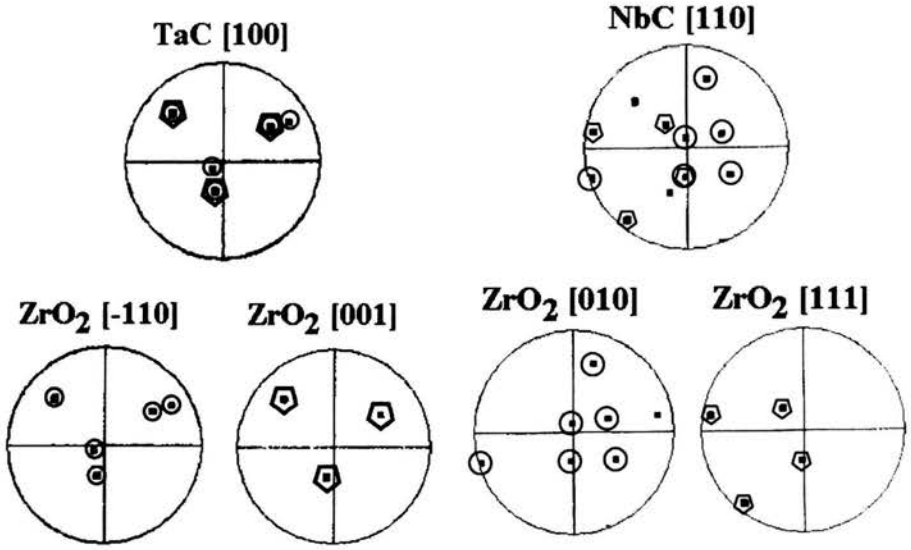

Fig. 17. Stereographic projections of the crystallographic directions on the plane of the sample surface: [$\bar{1}$10], [001] of Y-TZP and [100] of neighboring TaC grain; [010], [111] of Y-TZP and [110] of neighboring NbC grain

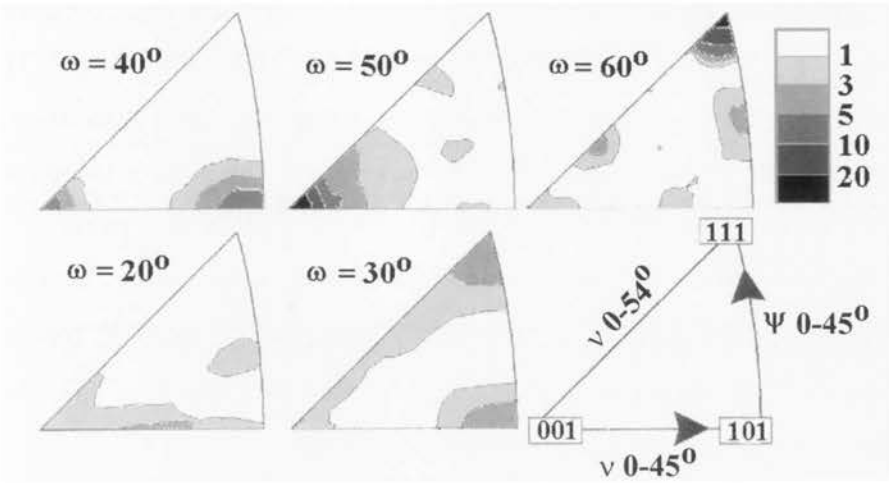

Fig. 18. Misorientation distribution function calculated from a set of ≈7500 misorientations between the neighbouring Y-TZP and NbC grains. Positions of rotation axis given in spherical polar coordinates (υ, ψ) reduced to a spherical standard triangle

These are typical examples (chosen from dozens of already measured) of the crystal direction arrangements in two neighbouring grains of different phases. It can be noticed that the crystallographic relationships established independently by SAED and EBSD are not the same. However, it is believed that this is only a matter of improved statistics and further analysis of larger areas of the composites to find identical correlations as it was in the case of the alumina/WC and Y-TZP/WC system.

The stereographical projections presented in Fig. 18 suggest that zirconia and carbides adjacent grains are not arranged in a random way. For all pairs of grains in the Y-TZP/TaC and Y-TZP/NbC systems, misorientations, described in the axis–angle space by the rotation axis **r**, common to both adjacent crystallites, and rotation angle **ω**, have also

been calculated. By rotation of angle ω around the **r** axis the coordinate system of the first crystallite is transferred into the other. The misorientations are described statistically using the three-dimensional misorientation distribution function [19]. From the calculated misorientation distribution function for the Y-TZP/NbC system it is clearly seen that the dominating orientation relationship between neighbouring NbC and ZrO_2 grains can be described by ≈40-45° rotation around the [001] direction, ≈30-40° around the [101] direction and ≈60° rotation around the [111] direction (twin rotation).

A very similar orientation relationship was observed between neighbouring TaC and ZrO_2 grains.

4. Conclusion

A co-precipitation method enables to produce TZP/Al_2O_3 composites with alumina particulates of a near-nanometric size and narrow size distribution. Morphology of a starting alumina powder and an applied mixing route controls inclusion size distributions in composites obtained by the physical mixing method.

A nanometric size of alumina particulate is not a critical factor controlling mechanical properties of the TZP/Al_2O_3 composites with intergranular inclusions. It is density of the composite and a size of microstructural defects.

The TZP/Al_2O_3 composites containing 5 vol.% of submicronic alumina particulate inclusions can reach fracture strength of 1.7±0.2 GPa at a density of 99.0±0.2 %.

TEM and EBSD were successfully used to analyse alumina/ WC, Y-TZP/WC, Y-TZP/NbC and Y-TZP/TaC composite. Crystal relationships between the zirconia matrix and particulate reinforcing additive were established not only in local areas but also in the global volume. The EBSD technique confirmed the orientation relationships observed by TEM in the alumina/ WC and Y-TZP/WC composites. However, in case of the Y-TZP/NbC and Y-TZP/TaC composites the crystallographic correlations measured by both methods were not always identical. Thus, a more advanced analysis of the orientation relationships between neighbouring grains of different phases is necessary.

Charging problems were overcome by very carefully polishing with colloidal silica and then depositing a very thin carbon coating. Though thermal etching in oxygen free atmosphere produced damage free surface, sample topography deteriorates Kikuchi band contrast, which limits the number of indexable patterns.

Acknowledgement

Financial support has been provided by AGH - University of Science and Technology under the project *11.11.160.111* and the Polish Committee for Scientific Research under a grant 3T08D 020 26 for making the first part of this work.

References

1. Lee W.E., Rainforth W.M., Ceramics Microstructures – Property Control by Processing, Chapter 9.1.1., Chapman & Hall, London, 1994.

2. Tsukuma K., Ueda K, Shimada M, Strength and Fracture Toughness of Isostatically Hot-Pressed Composites of Al_2O_3 and Y_2O_3-Partially-Stabilized ZrO_2, J. Am. Ceram. Soc., 1982, 68, C-4 – C-5.
3. Haberko K., Pędzich Z., Róg G., Bućko M.M., Faryna M, The TZP matrix-WC particulate composites, *Eur. J. Solid State Inorg. Chem.*, 1995, 32, 593.
4. Hannink, R.H.J., Kelly, P.M. Muddle, B.C., Transformation toughening in zirconia-containing ceramics, J.Am.Ceram.Soc. 2000, 83, 461-487.
5. Pędzich Z., Haberko K., Toughening mechanisms in the TZP-WC particulate composites, Key Eng. Mater. 1997, 132-136, 2076-2079
6. Rejendran S., Rossell H.J., Sanders J.V., Preparation and characterization of precursors powders for yttria-doped tetragonal zirconia polycrystals (Y-TZP) and Y-TZP/Al_2O_3 composites, J. Mater. Sci., 24, 1989, 1195-1202.
7. der Exter P., Winnubst A.J.A., Burggraaf A.J., The preparation and characterization of Y-TZP/20 vol.% Al_2O_3, J. Euro. Ceram. Soc., 11, 1993, 497-507.
8. Shi J.L., Li B.S., Ruan M.L., Yen T.S., Processing of Nano-Y-TZP/Al_2O_3 Composites. I: Preparation and Characterization of Nano-Y-TZP/Al_2O_3 Composite Powders, J. Euro. Ceram. Soc., 15, 1995, 959-965.
9. Sternitzke, M., Review: Structural ceramic nanocomposites, J.Eur.Cer.Soc., 17 (1997) 1061-1082.
10. Mecartney M.L., Influence of an amorphous second phase on the properties of yttria-stabilised tetragonal zirconia polycrystals (Y-TZP), J. Am. Ceram. Soc., 1987, 70, 54-58.
11. Lawn B., *Fracture of Brittle Solids*, II edition, Cambridge, UK, 1993.
12. Lange F.F., Processing-Related Fracture Origins: I, Observations in sintered and isostatically hot-pressed Al_2O_3/ZrO_2 composites, J. Am. Ceram. Soc., 66, [6], 1983, 396-398.
13. Fukuhara M., Properties of (Y)ZrO_2-Al_2O_3 and (Y)ZrO_2-Al_2O_3-(Ti or Si)C Composites, J. Am. Ceram. Soc., 1989, 72, 236-242.
14. D.J. Dingley, V. Randle, Review: Microtexture determination by electron back-scatter diffraction, J. Mater. Sci., 1992, 27, 4545.

15. R. Schwarzer, Review: Automated crystal lattice orientation mapping using a computer-controlled SEM, Micron, 1997, 3, 249.
16. F.J. Humphreys, Review: Grain and subgrain characterisation by electron backscatter diffraction, J. Mater. Sci. 2001, 36, 3833.
17. D. Katrakova, F. Mücklich, Specimen preparation for electron backscatter diffraction (EBSD) – part II: Ceramics, Prakt. Metallogr., 2002, 39, (12), 644.
18. M. Faryna, E. Bischoff, K. Sztwiertnia, Crystal orientation mapping applied to the Y-TZP/WC composite, Mikrochim. Acta, 2002, 139, 55.
19. J.Pośpiech, K.Sztwiertnia, F.Haessner, Textures Microstruct. 6 (1986) 201.